THE JOURNAL OF PHYSICAL CHEMISTRY B

Article

Cite This: J. Phys. Chem. B 2019, 123, 266−276

pubs.acs.org/JPCB

Drying Kinetics of Salt Solution Droplets: Water Evaporation Rates and Crystallization

F. K. A. Gregson,[†] J. F. Robinson,[‡] R. E. H. Miles,[†] C. P. Royall,[†,‡] and J. P. Reid*[,†]

[†]School of Chemistry and [‡]School of Physics, University of Bristol, Bristol BS8 1TS, U.K.

Supporting Information

ABSTRACT: Drying and crystallization of solution droplets is a problem of broad relevance, determining the microstructures of particles formed in spray-drying, the phase of particles delivered by, for example, aerosol formulations for inhalation therapies, and the impact of aerosols on radiative forcing and climate. The ephemeral nature of free droplets, particularly when considering the drying kinetics of droplets with highly volatile constituents, has often precluded the accurate measurement of transient properties such as droplet size and composition, preventing the robust assessment of predictive models of droplet-drying rates, nucleation, and crystallization. Here, we report novel measurements of the drying kinetics of individual aqueous sodium chloride solution droplets using an electrodynamic balance to isolate and trap single aerosol droplets (radius ≈ 25 μm). The initial solution droplet size and composition are shown to be highly reproducible in terms of drying rate and crystallization time when examined over hundreds of identical evaporating droplets. We introduce a numerical model that determines the concentration gradient across the radial profile of the droplet as it dries, considering both the surface recession because of evaporation and the diffusion of components within the droplet. Drying-induced crystallization is shown to be fully determined for this system, with nucleation and instantaneous crystallization occurring once a critical supersaturation level of 2.04 ± 0.02 is achieved at the surface of the evaporating droplet. This phenomenological model provides a consistent account of the timescale and surface concentration of free-droplet crystallization on drying for the different drying conditions studied, a necessary step in progress toward achieving control over rates of crystallization and the competitive formation of amorphous particles.

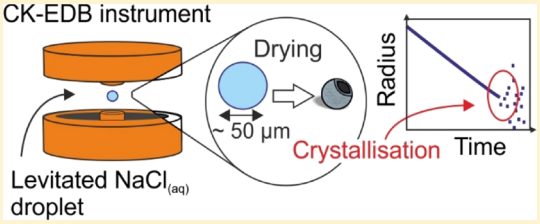

INTRODUCTION

Drying of liquid droplets to form particles is an important process for a range of industries, from agriculture and inkjet printing to the production of pharmaceutics, cosmetics, and food.[1−4] In addition, the propensity of an aerosol droplet to crystallize into solid particles has been shown to dramatically influence the optical properties of atmospheric aerosols and, thus, their radiative forcing.[5,6] The evolving heterogeneities in the particle microstructure as a droplet evaporates can be a highly complex process. Heat and mass transfer can be strongly coupled.[7] The competition between surface recession and internal flows such as convection, diffusion, and Marangoni flows can result in an array of product morphologies, size, and properties.[8−10] For some solutes, nucleation and crystallization is sufficiently rapid that dry crystalline particles result, depending on the drying rate; for other systems, drying may lead to amorphous glassy particles.[11,12] The crystallization of solutes present in a droplet is often the ultimate outcome of droplet-drying processes. The time at which nucleation occurs within an evaporating droplet can be directly linked to the initial droplet size and solute concentration, allowing some control over the final crystalline particle size and morphology. Our objective here is to examine the drying kinetics and crystallization of inorganic solution droplets. Through refined measurements of the drying rates of individual droplets, we will show that the crystallization time and surface composition at crystallization are highly reproducible over ranges of starting droplet composition and temperature, providing a phenomenological model for predicting the formation of crystalline particles.

Although there has been considerable work on the study of droplet drying on surfaces, that is, sessile droplets,[13−15] far fewer studies have examined the drying kinetics and crystallization of free droplets or aerosols. There are numerous unique experimental challenges associated with studying the drying dynamics of free droplets that are easily overcome when examining sessile droplets. Free droplets are ephemeral and difficult to follow in position unless a single particle is isolated and captured, such as with an optical trap,[16] electrodynamic balance (EDB),[17] or acoustic trap.[18] Even then, the timescales of evaporation processes can be <1 s, presenting a significant challenge to infer characteristic properties (e.g., size and composition at the point of crystallization) on such short timescales. Ensuring reproducibility in droplet generation and drying events is also crucial if sufficient statistics are to be achieved to infer the key microphysical details of the drying process. Finally, sampling the particles for off-line structural analysis requires deposition, which may also lead to a phase

Received: October 1, 2018
Revised: December 14, 2018
Published: December 14, 2018

DOI: 10.1021/acs.jpcb.8b09584
J. Phys. Chem. B 2019, 123, 266−276

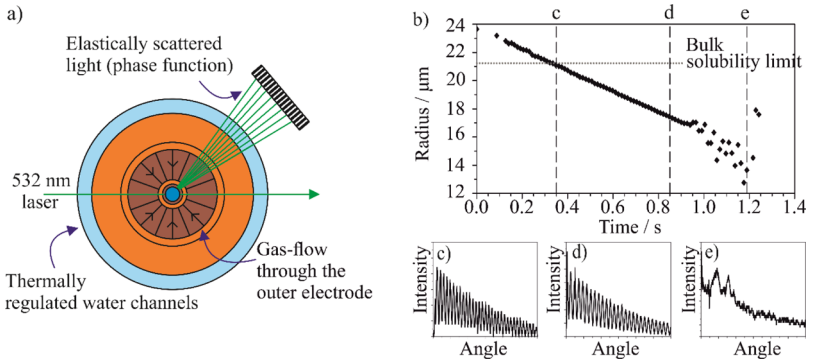

Figure 1. (a) Schematic of the electrodynamic balance double-cylindrical electrode system, as viewed from above. The gas flow passes through the electrode vertically and out of the page as shown. (b) Change in the radius with time of a levitated aqueous NaCl droplet (initial concentration 20% w/w) as it evaporates within the EDB. (c) Elastically scattered light (phase function) collected at 0.35 s; (d) at 0.85 s; (e) at 1.2 s.

change or change in particle composition.[19] However, studying free-droplet evaporation removes the complexities of the substrate−droplet interactions and Marangoni flows that occur for sessile droplets. In addition, the absence of a surface simplifies the symmetry for modeling, reduces the possibility of heterogeneous nucleation, and limits the treatment of heat transfer to conduction into the vapor phase. Free-droplet drying in air is also more representative of industrial processes such as crop-spraying and spray-drying. Thus, a greater understanding of how the particle formation process can be predicted and controlled would be integral to improving the efficacy of many industrial drying processes.

Spray-drying is the process of rapidly drying a stream of aerosolised solution droplets in a hot air flow, such that micrometer-sized particles are formed. Its application in many industries can be attributed to the speed and efficiency of the one-step process, and the short residence time of the droplets enables the use of heat-sensitive precursor compounds.[20] Although widely used, the process of particle formation from aerosol droplets is an active area of research as it is highly condition-dependent.[21] A better understanding of the factors governing the evaporation kinetics and how compositional heterogeneity develops within an evaporating droplet is critical to allow ultimate fine-tuning of drying conditions and precursor components and to deliver tailored final dry particles with desired characteristics.[22] Within a spray drier, droplet evaporation is typically rapid, that is, on timescales on the order of milliseconds to seconds. The rate of evaporation can outcompete the rate of diffusional solute mixing, leading to the enrichment of solutes at the droplet surface; the rate at which the solvent is replenished at the surface is much slower than the rate of surface recession. The Peclet number (Pe) is used to provide a measure of the ratio between the diffusion rate within a particle and the evaporation rate

$$Pe = \frac{\kappa}{8D_i} \tag{1}$$

where κ is the evaporation rate and D_i is the molecular diffusion coefficient of species i within a particle.[23] A Peclet number lower than 1 indicates that a homogeneous composition is maintained throughout the drying process; the diffusional mixing is fast enough to replenish the surface with solvent from the droplet bulk. However, Pe greater than 1 indicates that the surface is likely to become enriched as the droplet dries, with the surface receding at a greater rate than the time scale for diffusional mixing.[24−26]

In the bulk phase, crystallization of solutes typically occurs upon reaching saturation. However, metastable supersaturated solute states are prevalent in the aerosol phase, with crystallization only occurring at high solute concentration and a water activity much lower than the solubility limit, often referred to as the efflorescence point. Classical nucleation theory is built on an interplay between the interfacial free energy of the crystal-liquid phase boundary and the chemical potential difference between the liquid and crystalline phases.[27] The chemical potential difference rises with the increasing level of saturation within the droplet, and the interfacial free energy acts as a barrier to formation of a crystal nucleus. Although surfaces and impurities, such as dust, can act as heterogeneous nucleation sites and reduce the free energy barrier to nucleation, the absence of a solid surface enables an aerosol droplet to reach very high levels of supersaturation before efflorescence occurs. Typically, inorganic solutions effloresce at a water activity reported in terms of the gas-phase moisture content or the efflorescence relative humidity (ERH). At atmospheric temperature and pressure, the aerosol is only able to hold the salt in the aqueous solution form under conditions of higher moisture content than the ERH. Homogeneous nucleation is a rare event, and the stochastic nature means that efflorescence is typically reported over an RH range as there is inherent randomness in the occurrence of nucleation.[28] For sodium chloride, this range is narrow, and while size dependence of the droplet on the ERH has been reported,[29] the ERH for droplets of the size range in this work is reported to be 44−45% RH.[30] A water activity of 0.45 corresponds to a molality of 12.68 mol kg^{-1}, a concentration of 648 g L^{-1}, and a supersaturation level of 2.04.[31]

A series of studies have investigated the drying of inorganic solution droplets evaporating both on surfaces and during levitation, inferring the nucleation rate as a function of the supersaturation level reached.[32,33] We focus here on the crystallization of evaporating sodium chloride droplets. Aqueous sodium chloride was chosen as the system for study as the thermodynamic equilibrium behavior of aqueous sodium chloride aerosol is well-characterized,[31] and the evaporation of water from aqueous NaCl sessile droplets has been studied in detail.[13,34] Sodium chloride is also a common precursor compound used industrially. It is particularly prevalent in the preparation of food, and its particle formation process is relevant because of a drive to reduce salt intake in populations.[35] There have been reports stating that one can increase the intensity of salt flavor by adjusting particle size and

DOI: 10.1021/acs.jpcb.8b09584
J. Phys. Chem. B 2019, 123, 266−276

morphology, allowing an overall lower mass of NaCl to be used.[36,37] In addition, NaCl is a large component of sea spray, and thus, it is important to understand its crystallization and phase behavior for climate models.[38]

In this work, we report measurements of the time-dependent radius of a rapidly evaporating sodium chloride droplet throughout the drying process and the time of crystallization. Trapping the droplet in free air while it dries eliminates any heterogeneous nucleation site such as a container wall and only the homogeneous nucleation of NaCl crystals is probed. These measurements are performed on a large population of droplets, providing a comprehensive statistical analysis on the propensity to crystallize. Homogeneous nucleation of NaCl occurs above a certain critical supersaturation, S_c. The evaporation kinetic results are compared with simulations of the evolving internal concentration gradients within the evaporating droplets.

EXPERIMENTAL METHOD AND ASSESSMENT OF THE PARTICLE PHASE STATE

The evaporation of water from sodium chloride solution droplets was studied using the EDB (see Figure 1a). In all experiments, HPLC-grade water and BioXtra ≥99.5% NaCl (Sigma-Aldrich) were used. The EDB instrument has been described in detail in previous work[39] and will only be briefly reviewed here. A droplet-on-demand generator is used to produce a single droplet of known composition which is charged (<10 fC, e.g., from an imbalance in Na^+ and Cl^-) and injected into the EDB trapping chamber. An ac voltage is applied to a pair of upper and lower concentric cylindrical electrodes, generating an electric field in which the droplet is trapped. The gravitational and drag forces acting on the droplet are offset by a dc voltage applied to the bottom electrode. A flow of dry nitrogen passes over the trapped particle at a rate of 0.03 m/s, and the trap temperature (273–323 K) is controlled by circulating ethylene glycol coolant through the electrodes.

The droplet is illuminated with a 532 nm CW laser, and the resulting elastically scattered light pattern (phase function) is collected over an ∼24° angular range centered at 45° to the forward direction of the laser (see Figure 1b). During the time period that the trapped droplet is homogeneous and spherical, it produces regularly spaced interference fringes in the phase function which allow the size of the droplet to be calculated. The angular separation between the light and dark fringes in the phase function is used to calculate the droplet radius, R, using the geometric optics approximation to Mie theory.

$$R = \frac{\lambda}{\Delta\vartheta}\left(\cos\left(\frac{\vartheta}{2}\right) + \frac{n\sin\left(\frac{\vartheta}{2}\right)}{\sqrt{1 + n^2 - 2n\cos\left(\frac{\vartheta}{2}\right)}}\right)^{-1} \quad (2)$$

where λ is the laser wavelength, ϑ is the central viewing angle, $\Delta\vartheta$ is the angular separation between the fringes, and n is the droplet refractive index. This approximation can allow the determination of the droplet radius with an accuracy of ±100 nm.

The concentration in g L^{-1} averaged across the droplet volume is calculated as a function of time using the droplet volume, obtained from the radius measurement, and the dry mass of NaCl, which is known from the starting concentration. As the concentration of the aqueous NaCl droplets increases and the water evaporates, radius data are corrected for the time-dependent change in droplet refractive index in a postanalysis step.[39] The refractive index of the droplet at all times can be calculated from the concentration using the molar refraction mixing rule.[40] This method assumes that the droplet composition is homogeneous, which is unlikely to be the case; rapid evaporation may lead to surface enrichment and an inhomogeneous droplet. Hence, there is an uncertainty in the radius resulting from the refractive index estimation, which increases as the droplet surface becomes more enriched. The error resulting from this is estimated in the Supporting Information. Even an appreciable surface enrichment does not significantly affect the refractive index and only begins to affect the estimate of the radius in the last ∼0.1 s of the droplet lifetime where the error in the radius remains less than 5%. The experimentally determined crystallization times are unaffected.

Crystal nucleation occurring within the droplet leads to a sudden lack of homogeneity in composition and shape, which is detectable from a dramatic change in the form of the phase function. The spacing of the interference fringes becomes highly erratic and the particle size can no longer be inferred (see Figure 1b). The sensitivity of the EDB measurement for detecting the efflorescence time is therefore the minimum interval at which the phase function is recorded, which is typically 10 ms. This method can only identify the time frame at which particle crystallization occurs, based on the dramatic changes in light scattering observed in the phase function; the method is unable to identify the time at which nucleation occurs. This method of identifying the point of efflorescence has previously been used to detect nucleation events in levitated aqueous NaCl droplets as they evaporate slowly in equilibrium experiments[41] and also to observe ice nucleation events in homogeneous freezing experiments of sulfuric acid solution droplets.[42] The point of nucleation was determined to be the moment where the fringe diffraction pattern characteristic of a spherical droplet was lost from the elastic light scattering, leaving an incoherent speckle pattern. In this work, when slow step-wise changes in RH are made, progressively drying the droplet to lower water activity, the loss of the regular scattering pattern occurred at a water activity of 0.45, consistent with previous efflorescence studies that report an efflorescence RH of 45% for NaCl,[43] thus validating the method for efflorescence detection.

Further conclusive evidence that crystallization occurs when an aqueous NaCl droplet evaporates into dry nitrogen is provided in Figure 2. In both measurements shown, the solution droplets crystallize after ∼1.7 s of evaporation. Then, for one of the particles, the RH was increased to ∼85% approximately 30 s into the experiment, increasing the gas-phase water content above the deliquescence RH of 75%.[31] As anticipated, the NaCl particle dissolved, water condensed, and the particle became a homogeneous solution droplet allowing a precise measurement of size after t = 150 s. Conversely, the RH surrounding a second crystallized particle was increased to 63%, that is, below the deliquescence RH. In this case, the particle remained crystalline, precluding a precise determination of particle radius using the phase function. The presence of a deliquescence transition at RH > 75% confirms that the transition at RH < 45% observed is indeed efflorescence.

DOI: 10.1021/acs.jpcb.8b09584
J. Phys. Chem. B 2019, 123, 266–276

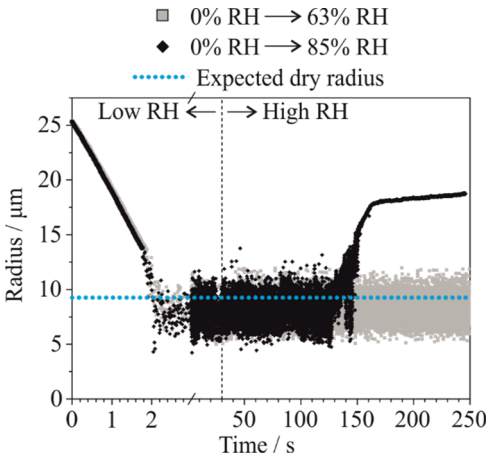

Figure 2. Evaporation of two aqueous NaCl droplets (initial concentration 10% w/w) into dry nitrogen, leading to efflorescence at t = 1.7 s. The RH is increased to a higher RH after 30 s into the experiment. When the humidity is increased to 85% RH (black points), the crystalline particle absorbed water and subsequently deliquesced at approximately t = 150 s. When the RH is increased only to 63% (gray points), deliquescence is not observed, and the particle remained in the crystalline form. Also shown is the effective spherical radius of the solid NaCl particle estimated from the initial solution droplet wet size and solute concentration.

RESULTS AND DISCUSSION

The time taken for an evaporating aqueous NaCl droplet to effloresce was recorded for large populations of droplets at different gas-phase temperatures. Thus, only data acquired (and averaged) over many droplets are reported below unless otherwise stated. First, we consider the reproducibility of the efflorescence behavior of evaporating aqueous NaCl droplets. Second, the impact of changing the gas-phase temperature and initial concentration on the efflorescence time is reported. The volume-averaged concentration of the evaporating droplets as a function of time is presented and discussed along with estimates of the respective Peclet numbers for each set of evaporation conditions. We then introduce a model that maps the evolving internal microstructure of the droplets, presenting the model predictions of droplet surface concentrations which are in good agreement with the experimental observations of the crystallization times of the droplets.

Reproducibility of Efflorescence Events across Populations of Droplets. To demonstrate the reproducibility of the efflorescence events when measuring the kinetics of droplet evaporation, the drying profiles of 230 NaCl droplets evaporating into dry air at 293 K were recorded and the results are shown in Figure 3a. The data demonstrate both the reproducibility in the droplet size generated by the droplet dispenser (24.0 μm $\pm$ 0.1) as well as the reproducibility in the timing of the efflorescence event, characterized by the point at which the radius can no longer be calculated using the optical fringes in the phase function. In Figure 3a, this occurred at 0.95 $\pm$ 0.02 s following droplet generation. This equates to a solute concentration averaged over the droplet volume of 636 $\pm$ 7 g L^{-1}. The microdispenser that produces single droplets is external to the EDB instrument and it requires approximately 0.2 s for the droplet to travel into the center of the chamber where it becomes trapped. Thus, the data points shown at t = 0 result from a back extrapolation from the time dependence of the square of the radius at the earliest times after the droplet is captured in the trap.

Effect of the Evaporation Rate on Efflorescence Time. The evaporation rate of an aqueous sodium chloride droplet in dry nitrogen depends on two factors: the gas-phase temperature and the solute concentration in the initial droplet. Increasing the gas-phase temperature, or decreasing the solute concentration, leads to a higher droplet evaporation rate due to the resulting increase in the vapor pressure of solvating water present in the droplet. Conversely, an increase in solute concentration suppresses the vapor pressure of water and slows the evaporation rate. The consequences of changing the gas-phase temperature within the EDB chamber for the efflorescence time are shown in the histogram in Figure 3b.

First, it should be noted that the distribution in efflorescence time at each temperature is narrow, showing the reproducibility in the efflorescence behavior of aqueous sodium chloride as a system. Previous reports have suggested that homogeneous nucleation is a stochastic process, with close fits of data of homogeneous nucleation at a specific level of supersaturation to Poisson distributions.[44] However, the distributions in efflorescence time in this work, as shown in Figure 3b, cannot be presented as a probability of nucleation occurring as a function of induction time at a specific defined supersaturation level, as in the work of Durán-Olivencia et al.[44] Rather, in this work, the droplets are exposed to rapidly increasing levels of supersaturation, and thus, the "induction time" cannot be readily defined.

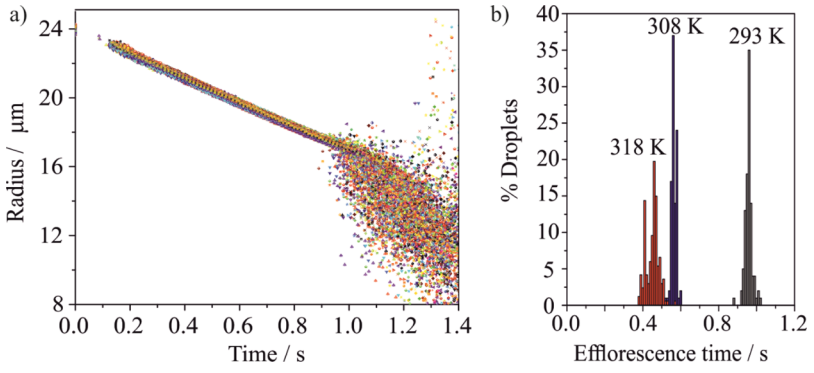

Figure 3. (a) Overlaid evaporation profiles of 230 aqueous NaCl droplets (20% w/w) evaporating into dry air at 293 K. (b) Distribution in efflorescence times observed at different gas-phase temperatures for a large population of droplets (upwards of 200 in each case). Efflorescence time is defined as the time from the creation of the droplet until efflorescence is detected in the EDB.

DOI: 10.1021/acs.jpcb.8b09584
J. Phys. Chem. B 2019, 123, 266−276

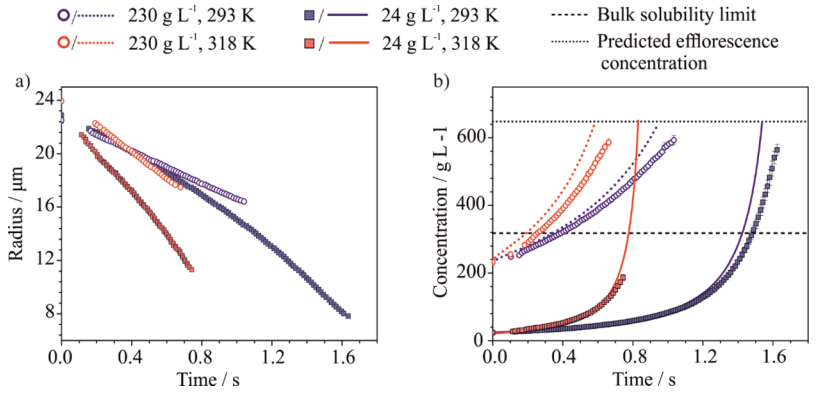

Figure 4. (a) Change in radius with time of aqueous NaCl droplets with different initial solute concentrations evaporating into dry nitrogen at different temperatures. Data points show experimental data averaged over a minimum of 10 droplets. Error bars are smaller than the data points. (b) Change in the volume-averaged concentration of NaCl within the evaporating droplets as a function of time inferred from the experimental measurements of radius (points). The solubility limit in the bulk phase and the predicted efflorescence concentration from slow drying measurements are indicated by the horizontal lines. Data points show experimental data averaged over a minimum of 10 droplets. Solid and dotted lines show the surface concentration as predicted by the model.

Table 1. Recorded Efflorescence Times and Final Averaged Concentrations (Averaged over a Minimum of 15 Droplets) for Different Initial Solute Concentrations of Aqueous NaCl Droplets and Different Gas-Phase Temperatures

initial feed concentration of NaCl/g L^{-1}	gas-phase temperature/K	volume-averaged efflorescence concentration/g L^{-1}	efflorescence time/s	initial Peclet number
24	293	630 ± 10	1.51 ± 0.02	0.023
24	318	200 ± 20	0.74 ± 0.03	0.037
230	293	636 ± 7	0.95 ± 0.02	0.054
230	318	640 ± 20	0.45 ± 0.03	0.082

Second, the timescale for particle efflorescence is observed to decrease as the gas-phase temperature increases, falling from 0.95 ± 0.02 s at 293 K to 0.56 ± 0.01 s at 308 K and 0.45 ± 0.03 s at 318 K. The higher gas-phase temperature leads to more rapid evaporation because of the increase in water vapor pressure and a rise in solute concentration and saturation to the point where nucleation and crystallization occurs at an earlier time in drying. In an analogous way, the impact of changing the starting concentration of NaCl in the aqueous droplet on the evaporation rate is also shown in Figure 4a. The droplet with a higher starting concentration of NaCl (230 g L^{-1}) has a lower water vapor pressure and, thus, a slower evaporation rate than the 24 g L^{-1} NaCl droplet. Despite the slower evaporation rate for the more concentrated droplet, efflorescence still occurs earlier into the droplet lifetime for the higher initial concentration at both temperatures. The greater concentration in the initial droplet ensures that the critical supersaturation level for efflorescence to occur is reached earlier into the droplet lifetime.

Volume-Averaged Concentration of Evaporating Droplets. For the four drying conditions shown in Figure 4a, the volume-averaged concentration of NaCl in each droplet was calculated, assuming a homogeneous composition and spherical shape, and the results are shown in Figure 4b. The recorded efflorescence times and the volume-averaged concentration for the different drying conditions are reported in Table 1. Three of the four datasets indicate that the droplets effloresced at average NaCl concentrations above the bulk solubility limit but below the required supersaturation expected from previous measurements of the efflorescence RH. However, for the case of the initial NaCl feed concentration of 24 g L^{-1} and temperature of 318 K, the droplets effloresced at 0.74 ± 0.03 s after the droplet was dispensed. This equates to a volume-averaged concentration at the point of efflorescence of 200 ± 20 g L^{-1}, which is below even the bulk solubility limit of NaCl of 318 g L^{-1}. This indicates that crystallization of the evaporating droplets cannot be triggered by processes in the droplet bulk as the solute supersaturation never achieves a sufficiently high value. We propose instead that the rapid evaporation of the droplets leads to a surface enrichment of solute, which exceeds the nucleation supersaturation. This leads to crystallization at the droplet surface while the volume-averaged concentration remains low. Thus, we must not assume that complete crystallization has taken place in the droplet immediately at the time that the light-scattering phase function suggests the particle is no longer spherical. However, the fully dry gas phase will lead to the irreversible and complete loss of water from the droplet, and a fully crystalline particle must form soon after crystallization begins, even though this second stage of drying is not clearly resolvable in our measurements.

Increasing the gas phase, and thus the droplet, temperature increases the evaporation rate, while also increasing the binary diffusion coefficient of water within the droplet according to the Stokes−Einstein relationship

$$\frac{D_1}{D_2} = \frac{T_1}{T_2}\frac{\mu_2}{\mu_1} \tag{3}$$

where D_T is the binary diffusion coefficient at temperature T, and μ_T is the dynamic viscosity of the solvent (assumed to remain constant between 293 and 318 K for aqueous NaCl solutions). Increasing the temperature also increases the bulk solubility of inorganic salts, although this is only a small increase, from 317.5 g L^{-1} at 293 K to 321.7 g L^{-1} at 318 K, for NaCl.[45] The observation that the droplets at higher temperatures effloresce earlier than those at lower temperatures

DOI: 10.1021/acs.jpcb.8b09584
J. Phys. Chem. B 2019, 123, 266−276

suggests that the increase in the evaporation rate from 293 to 318 K is sufficiently large that the surface supersaturation required for nucleation is achieved earlier in the evaporation process, outcompeting the increase in the binary diffusion coefficient. Quantitatively, the average evaporation rate increases from 2.52 ± 0.01 × 10^{-10} m^2 s^{-1} at 293 K to 4.2 ± 0.1 × 10^{-10} m^2 s^{-1} at 318 K (a 66% increase); over this compositional range, the binary diffusion coefficient is increased by 8.5% at the higher temperature (see eq 3). Thus, in this instance, observing efflorescence at earlier time when increasing the temperature is consistent with expectations from the Peclet model.

The Peclet number at $t = 0$ s for the four datasets is shown in Table 1, as calculated using eq 1. All four datasets show Peclet numbers that are well below 1, which would suggest that the initial binary diffusion coefficient within the droplets is sufficiently large when compared to the evaporation rate to keep the droplet well mixed throughout the drying process, resulting in dense, homogeneous particles. However, the experimental data in Figure 4b suggest that crystallization must occur at the surface, induced by surface enrichment during drying, as the average efflorescence concentration is below the critical supersaturation level. Aqueous NaCl solutions have been shown to increase in viscosity by as much as 5 times between dilution and the solubility limit in the aerosol phase,[46] and, thus, the binary diffusion coefficient can be expected to decrease as the droplet evaporates. Taking this into account would imply that the binary diffusion coefficient near the surface would decrease, leading to greater surface enrichment as the aqueous NaCl droplet evaporates than a simple evaluation of the Peclet number with a single value of the diffusion coefficient suggests. We now explore the evolving concentration profiles within the evaporating droplets more closely.

Modeling the Internal Concentration Profiles of Evaporating Droplets. We present below an analysis of the internal concentration profile of the evaporating droplets, particularly examining the degree of supersaturation at the droplet surface throughout the evaporation process. We treat the droplet as a moving boundary problem which uses the experimentally determined evaporation rates at each time step to provide the rate of surface recession. The solute profile evolution is obtained by numerically integrating the diffusion equation using finite difference methods. The droplet is split into a series of radial shells with thickness ~20 nm from which the solute concentration is calculated.

More specifically, we model the binary fluid droplet as a sphere of outer radius $R(t)$, where the initially uniform solute concentration evolves according to a diffusion equation neglecting temperature and convection effects. The solute concentration profile $c(r, t)$ at distance $r \in [0, R]$ from the center-of-mass then evolves with spherical symmetry according to the nonlinear diffusion equation

$$\frac{\partial c}{\partial t} = \nabla\cdot(D\nabla c) \tag{4}$$

Our previous measurements of the viscosity of aqueous aerosol droplets of NaCl solutions at 293 K reported that the viscosity depends on solute concentration (water activity), indicating that the binary diffusion coefficient D would also be affected by the changing NaCl concentration in an evaporating aqueous droplet.[46] To examine this effect, we have estimated the value of the binary diffusion coefficient D across the NaCl concentration range at 293 K using the Stokes−Einstein relation, as detailed in the Supporting Information and accounted for by eq 3. Assuming a general Einstein form for the relationship of the binary diffusion coefficient to temperature (i.e., $D \propto k_B T$), we obtain values at arbitrary temperature using the scaling

$$D(T) = \frac{D(293\ \mathrm{K})}{293} T \tag{5}$$

The model does not consider the change in droplet temperature because of evaporative cooling, which is likely to cause a reduction to the diffusion coefficient at the droplet surface.

Only the solvent evaporates at the surface leaving a constant total solute mass within the droplet, imposing zero flux through the outer boundary. Together with a compatibility condition at $r = 0$, we obtain the complete set of boundary conditions for eq 4 as

$$\left.\frac{\partial c}{\partial r}\right|_{r=0} = 0 \tag{6a}$$

$$\left.\frac{\partial c}{\partial r}\right|_{r=R} = -\frac{c(R)}{D}\frac{\mathrm{d}R}{\mathrm{d}t} \tag{6b}$$

The evolution of the outer radius depends on the mass flow through the outer boundary and the local density $\rho(r)$, which is itself a function of the concentration profile. Mass conservation gives the radial evolution in terms of the evolution of the total mass $m(t)$ as

$$\frac{\mathrm{d}R}{\mathrm{d}t} = \frac{1}{\rho(R)R^2}\left(\frac{1}{4\pi}\frac{\mathrm{d}m}{\mathrm{d}t} - \int_0^R \frac{\partial \rho}{\partial t} r^2\, \mathrm{d}r\right) \tag{7}$$

which requires a model for the solvent evaporation $\mathrm{d}m/\mathrm{d}t$ for closure. Evaporation is modeled in similar experiments with the Kulmala model,[47] but in this work, where the dry air causes rapid evaporation rates, we find significant deviations from this semianalytic model. The Kulmala model assumes that the temperature change at the boundary is small: an assumption that breaks down with rapid evaporation. Instead, given our primary aim is to track the internal concentration field throughout the measurement and to investigate the factors governing crystallization, we fit the evolution of droplet sizes seen in the experiments with $R(t)^2 = R(0)^2 - 2\kappa t$, obtaining

$$\frac{\mathrm{d}R}{\mathrm{d}t} = \frac{\kappa}{R} \tag{8}$$

with which eqs 4, 6a, and 6b can be solved. Constraining the modeled mass flux to the measurements through assuming a linear fit to the time dependence in the square of the radius is a reasonable assumption until very close to the time at which crystallization is observed (within 0.1 s). This is shown in the Supporting Information in Figure S3.

To solve this moving boundary problem, it is convenient to transform into the coordinate system $\tilde{r} = r/R$ in which the domain is fixed in time and eq 4 acquires an effective flux term. In these coordinates, the system of eqs 4, 6a, 6b, and 6b is readily solved using a second-order integration scheme[48] for an initial uniform concentration profile. Microcapillary experiments[49] suggest that homogeneous nucleation for NaCl is almost instantaneous at a fixed supersaturation, so we integrate until the concentration at the outer boundary reaches a solute supersaturation cutoff value. We confirm the numerical

DOI: 10.1021/acs.jpcb.8b09584
J. Phys. Chem. B 2019, 123, 266−276

stability of the trajectories by varying the temporal and spatial resolutions over an order of magnitude, with no appreciable effect to the final result. As far as we are aware, there is no model that can accurately simulate the rapid evaporation and resulting microphysics, including crystallization, in an inorganic solution droplet in dry air. As outlined previously, the microphysics of such a drying droplet is highly complex because of the coupling between heat and mass transfer and the diffusional transport competing with evaporative flux. Hence, the model presented here is necessarily constrained to the experimentally determined evaporation rate to set a boundary condition. Future developments of this model would include a simulation of the evaporation, independent of experiments, to provide a predictive determination of the crystallization time in free-droplet drying.

The critical supersaturation value, S_c, at which efflorescence occurs has been measured experimentally by Desarnaud et al.[49] who reported homogeneous nucleation occurring in micro-capillaries at S_c = 1.6. Tang et al.[50] and Utoft et al.[51] reported S_c values of 1.87 and 1.9, respectively. Here, an S_c value of 2.04 ± 0.02 was used, based on calculations from the E-AIM model,[31] assuming a NaCl efflorescence RH of 45% equivalent to a solution with a water activity of 0.45. The values of efflorescence water activity of 0.45 and an associated error of ±0.01 are consistent with literature values of the efflorescence RH under slow evaporation conditions in a large number of aerosol measurements and our own experimental data.[30,31,52] Using the E-AIM model, the NaCl solute concentration at a gas-phase RH of 45% at 293 K is 648 g L^{-1}, that is, a molality of 12.68 mol kg^{-1} and a supersaturation value of 2.04. The model terminates when the concentration in any region within the evaporating droplet achieves this value of S_c, identifying the point at which crystallization is expected.

Validation for using the E-AIM-predicted value of S_c = 2.04 to terminate the model is provided in Figure 5. The figure shows the deviation between the measured crystallization time, $t_{measured}$, and the modeled crystallization time, t_{model}, as a function of the value of S_c used to terminate the model. The two measurements shown are those performed at 293 K, consistent with the thermodynamic model predictions from E-AIM, which are based on aerosol measurements performed at room temperature. A value of S_c = 2.04 ± 0.02 yields consistency between the modeled and experimental crystallization times for the two salt solution concentrations reported here. As we propose the critical efflorescence concentration to be the same for different conditions for NaCl, the value of S_c = 2.04 ± 0.02 is the only critical supersaturation for which the modeled t_{eff} matches the experimental t_{eff} within the experimental error. For measurements performed at 318 K, a value of S_c = 2.04 is still used. However, the increase in the NaCl bulk solubility limit with temperature, from 317.6 to 321.7 g L^{-1}, is explicitly included in the model when calculating supersaturation.

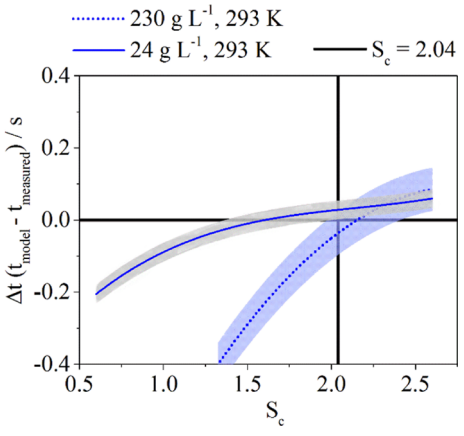

Figure 5. Deviation between the modeled crystallization time and that measured experimentally, as a function of the chosen value of the critical supersaturation S_c at which crystallization is assumed to occur. Previous aerosol-phase measurements involving slow step-wise decreases in RH at 293 K are consistent with a value for S_c of 2.04. This value yields congruent modeled and measured crystallization times for the droplet-drying measurements reported here starting from different initial salt concentrations, within the experimental error.

In Figure 6, we report the radial concentration profiles estimated as a function of time for droplets evaporating at different temperatures and starting solute concentrations, up until the point at which the nucleation supersaturation is exceeded in one of the radial shells. For all droplet compositions and gas-phase temperatures, the model predicts the highest solute concentration to be at the droplet surface, supporting the case for nucleation occurring at the particle surface. Changing the temperature and the initial solute concentration strongly influences how the radial concentration profiles evolve with time. Consider the two droplets evaporating at 293 K (Figure 6a,b): the droplet with the higher starting concentration exhibits a clear radial concentration gradient from the very beginning of the evaporation process, which increases in magnitude steadily until the nucleation supersaturation is exceeded at the surface and efflorescence occurs. By contrast, the droplet with the lower starting concentration does not initially show a radial concentration gradient and undergoes substantial evaporation before a significant gradient becomes evident. Even though the rate of surface recession (the evaporation rate) of the lower concentration droplet is more rapid, its initial solute concentration is so low that there is insufficient NaCl at early times to significantly enrich the surface as it recedes. However, by the point at which efflorescence occurs in the lower starting concentration droplet, the magnitude of its concentration gradient is more severe than that observed for the higher initial concentration droplet.

Increasing the temperature from 293 to 318 K causes a further increase in the magnitude of the radial concentration gradient, as shown in Figure 6c,d. For both starting concentrations, evaporation at 318 K leads to a much greater degree of surface enrichment in an evaporating droplet than at 293 K, because of the increase in their evaporation rates. This can be seen more clearly in Figure 4b. The corresponding lines show the calculated surface concentration of the droplets as a function of time, compared to the data points that show the volume-averaged concentration of the droplets from the experimental measurements. The internal concentration profiles for all four evaporation conditions show a positive deviation in the surface concentration away from the volume-averaged concentration, indicating surface enrichment. As discussed above, the two droplets with the higher starting concentration show this deviation from the beginning of the evaporation process, whereas the two droplets starting at 24 g L^{-1} have a surface concentration, that is, very similar to the average concentration, indicating a well-mixed droplet, until about 0.4 s into the droplet lifetime, at which time a sudden

DOI: 10.1021/acs.jpcb.8b09584
J. Phys. Chem. B 2019, 123, 266−276

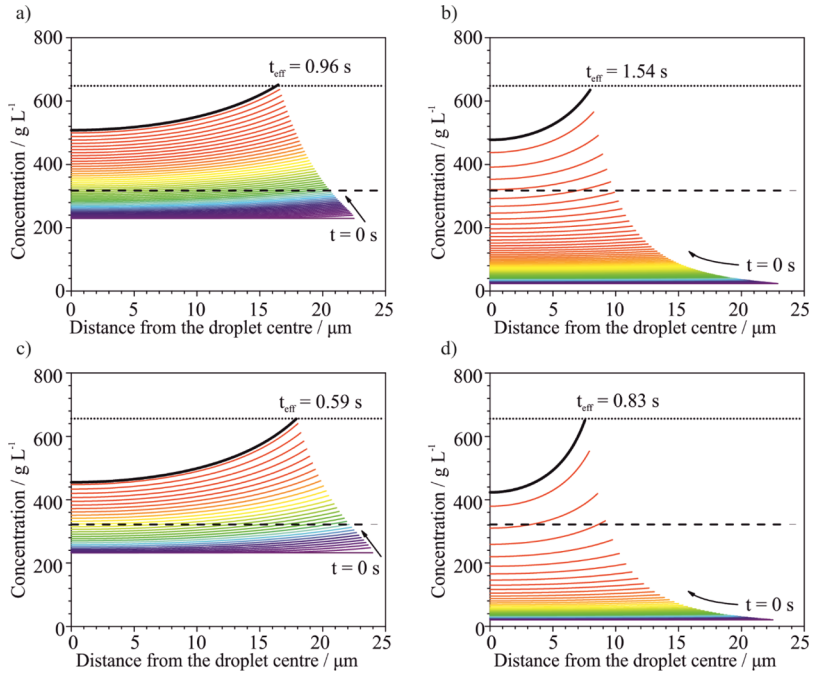

Figure 6. Radial concentration profiles within an evaporating NaCl droplet in dry air, at different initial concentrations and evaporating temperatures until the supersaturation level of 2.04 are reached. (a) Initial concentration of 230 g L^{-1} at 293 K; (b) 24 g L^{-1} at 293 K; (c) 230 g L^{-1} at 318 K; (d) 24 g L^{-1} at 318 K. Lines are at time steps of 0.02 s. The solid black line represents the radial concentration at the predicted efflorescence time (t_{eff}). Dashed black lines and dotted black lines are the bulk solubility limit and efflorescence supersaturation, respectively.

deviation from the averaged concentration line becomes apparent. The deviation is particularly large for the 24 g L^{-1} droplet evaporating at 318 K which shows the faster evaporation rate overall. At the time of efflorescence at ∼0.8 s, the difference between the surface concentration and the volume-averaged concentration is 260 g L^{-1}.

The radial concentrations at the point of crystallization for each droplet, and thus the degree of surface enrichment, are reported in Figure 7. The inset shows the time-dependent Peclet number, calculated with the experimentally determined evaporation rate and the composition-dependent binary diffusion coefficient value at the surface using eq 1. The binary diffusion coefficient as a function of concentration is provided in the Supporting Information and ranges from values on the order of 1 × 10^{-9} m^2 s^{-1} at the start of the evaporation process when the droplets are more dilute, down to values around 2 × 10^{-10} m^2 s^{-1} when the concentration of NaCl reaches 600 g L^{-1}. This causes the Peclet number to rise by almost an order of magnitude throughout the drying process. While the Peclet number for every droplet is initially very low, as shown in Table 1, the increasing viscosity as the droplet dries ultimately leads to compositional inhomogeneity across the radial profile. Crystallization occurs at a concentration closest to the volume-averaged supersaturation value predicted by the E-AIM model for the dataset with the least degree of surface enrichment at crystallization (a starting solute concentration of 230 g L^{-1} at 293 K). In addition, the dataset with droplets that exhibit the highest Peclet number at crystallization (the 24 g L^{-1} at 318 K case) shows a volume-averaged concentration that is furthest from the predicted level of supersaturation.

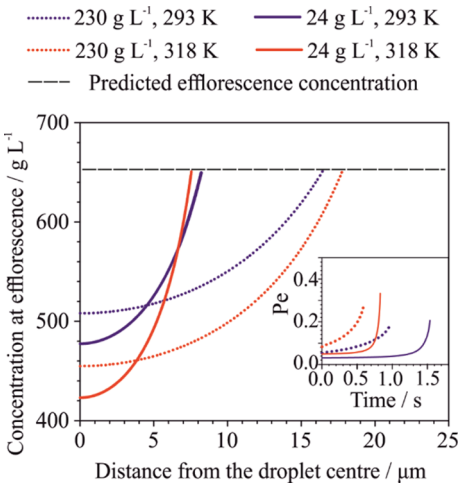

Figure 7. Radial concentration across the droplets at the predicted point of crystallization, showing the degree of surface enrichment at crystallization. Inset: The time-dependent Peclet number (Pe) for each of the droplets, calculated using the experimentally determined evaporation rate and the binary diffusion coefficient at the surface of the droplet, up until the point of model-predicted crystallization.

The experimentally observed crystallization times assuming a supersaturation of 2.04 at efflorescence, compared with those calculated using the model, are shown in Figure 8 and there is very good quantitative agreement. The modeled crystallization times for droplets evaporating into a gas phase at 293 K lie within the standard deviation of the measurements. For droplets evaporating into 318 K, crystallization in the model occurs slightly later than observed. It is possible that the magnitude of the evaporation rates at the higher temperature causes significant evaporative cooling to occur within the droplets, which would reduce the binary diffusion coefficient at the surface beyond what is currently accounted for and, thus, the Peclet number, and the extent of surface enrichment is likely to be higher than reported here.

DOI: 10.1021/acs.jpcb.8b09584
J. Phys. Chem. B 2019, 123, 266−276

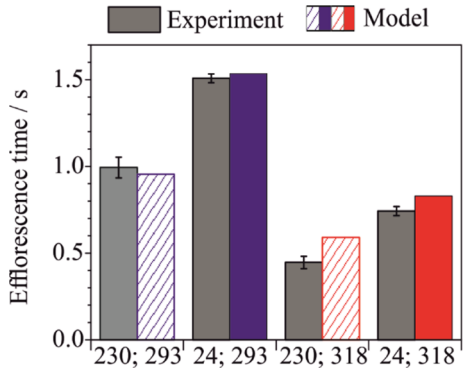

Figure 8. Comparison between experimentally determined efflorescence time of the droplets in the EDB and the efflorescence time as predicted by the model, for the different gas-phase temperatures and initial starting concentrations. The error bars in the experimental data correspond to the standard deviation in efflorescence times averaged over more than 100 droplets.

Our interpretation of the abrupt crystallization observed experimentally in terms of the developing radial concentration profile is critically dependent on choosing an appropriate value of the solute supersaturation at which crystallization occurs. S_c estimated from the E-AIM model was 2.04 ± 0.02; this model has been developed over many decades based on parameterizations to a large database of experimental data including bulk-phase measurements of osmotic coefficients up to the solubility limit of NaCl and, more crucially for this work, aerosol-phase measurements of hygroscopic growth measurements, deliquescence, and efflorescence.[31,53] However, we also must assume that the nucleation of crystals at both temperatures occurs instantaneously.

CONCLUSIONS

We have explored the evaporation kinetics of aqueous sodium chloride solutions, providing an ideal model system to study the crystallization of drying droplets and the dependence of the time required to achieve crystallization on the evaporation rate, as governed by the initial solute concentration and gas-phase temperature. Not only does NaCl show a remarkable degree of reproducibility, regarding the time at which identical droplets effloresce but also there is a clear dependence of the crystallization time on the temperature and evaporation rate. The internal concentration profiles at different radial points within the droplets are inferred using a Fickian integration model. Drying under all conditions investigated in this experiment led to droplets exhibiting an internal concentration gradient and an enriched solute concentration at the droplet surface. The basis for identifying solute crystallization is that NaCl achieves a particular level of solute supersaturation at which the nucleation rate of forming a crystal increases by orders of magnitude, such that nucleation becomes instantaneous.[49] When assuming this, a remarkable level of consistency is observed in interpreting the crystallization time across all drying environments investigated here, if crystallization is assumed to occur at a critical supersaturation of solute of 2.04 ± 0.02, a value that is always achieved first at the droplet surface.

On account of the consistency observed in the crystallization time of NaCl, it should be recognized that this represents an ideal system for benchmark studies. Not only are equilibrium compositions of aqueous solutions of NaCl (i.e., solute molality and molarity) with variation in water activity well established to very high solute supersaturation but also previous work has established accurate parameterizations for the solution density and refractive index to similarly high supersaturation, both essential for analyzing measurements. In addition, slow drying measurements on aerosol have provided an accurate indication of the water activity at efflorescence. Necessarily, we neglect any period between crust formation (the time at which the supersaturation is achieved) and termination of the drying process. However, this is not likely to be true for a wider range of inorganic and organic compounds. If an aerosol droplet enters conditions drier than the ERH, it still may not necessarily precipitate and certainly not immediately reaching a threshold saturation. There must always be an interplay between the nucleation rate and the drying rate. If a droplet evaporates very rapidly and the nucleation rate remains low, it is possible that the aerosol loses water more rapidly than crystal formation can occur and an amorphous solid would be formed. Under these circumstances, crystal nuclei may have insufficient time to form within the narrow precipitation window. The precipitation window begins when the surface of a droplet passes the bulk solubility limit, thus passing into the supersaturation regime and finishes when precipitation occurs within the droplet.[54] Efflorescence can occur at any point within this window.

Studies of the drying kinetics of aqueous spherical droplets avoid many of the complexities of studying the drying of droplets on a substrate. Droplets containing gradients in surface tension experience internal capillary flows from regions of low to high surface tension. This Marangoni effect is more prevalent in sessile droplets wherein the evaporation rate from different parts of the droplet is not constant, breaking the symmetry of the evaporating droplet and leading to concentration gradients along the surface profile. This in turn results in convection flows.[55] In aerosol droplets of aqueous NaCl, the spherically symmetric evaporation does not lead to such convections and, thus, Marangoni effects can be neglected. For a droplet of NaCl on a surface, the characteristic velocity of Marangoni flow has been reported to reach 4 m/s.[56] In such a system, the importance of this effect would have to be accounted for in a crystallization model. In addition, the temperature suppression at the surface of evaporating droplets because of the required latent heat can induce thermophoretic flow, out from the droplet center along the temperature gradient. While this effect would be small, it acts against the diffusional flow induced by concentration gradients.[57] At the drying rates studied here, we have neglected this thermophoretic effect, and this could be a contributing factor to the marginal overprediction of the crystallization time.

This work reports a step toward a greater understanding in the concentration profiles developing in evaporating free droplets and the first demonstration of the predictability in time and critical concentration of crystallizing aerosol. The concepts in this study can be developed for progress toward ultimately achieving product control in the crystallization of complex formulations and rapid drying applications such as spray-drying.

ASSOCIATED CONTENT

Supporting Information

The Supporting Information is available free of charge on the ACS Publications website at DOI: 10.1021/acs.jpcb.8b09584.

DOI: 10.1021/acs.jpcb.8b09584
J. Phys. Chem. B 2019, 123, 266−276

Discussion about the error in calculating the radius of the droplets caused by the surface enrichment, diffusion coefficients of aqueous NaCl as a function of concentration, applicability of using a linear fit to the time-dependent radius^2 for the evaporation rate, and method for determining the critical supersaturation for aqueous NaCl (PDF)

AUTHOR INFORMATION

Corresponding Author

*E-mail: j.p.reid@bristol.ac.uk.

ORCID

J. P. Reid: 0000-0001-6022-1778

Notes

The authors declare no competing financial interest.

ACKNOWLEDGMENTS

The authors acknowledge support from the Engineering and Physical Sciences Research Council under grant code EP/N025245/1.

REFERENCES

(1) Anyfantakis, M.; Geng, Z.; Morel, M.; Rudiuk, S.; Baigl, D. Modulation of the Coffee-Ring Effect in Particle/surfactant Mixtures: The Importance of Particle-Interface Interactions. *Langmuir* **2015**, *31*, 4113−4120.

(2) Liu, X.; Liu, W.; Carr, A. J.; Vazquez, D. S.; Nykypanchuk, D.; Majewski, P. W.; Routh, A. F.; Bhatia, S. R. Stratification during Evaporative Assembly of Multicomponent Nanoparticle Films. *J. Colloid Interface Sci.* **2018**, *515*, 70−77.

(3) Sear, R. P.; Warren, P. B. Diffusiophoresis in Nonadsorbing Polymer Solutions: The Asakura-Oosawa Model and Stratification in Drying Films. *Phys. Rev. E* **2017**, *96*, 062602.

(4) Gharsallaoui, A.; Roudaut, G.; Chambin, O.; Voilley, A.; Saurel, R. Applications of Spray-Drying in Microencapsulation of Food Ingredients: An Overview. *Food Res. Int.* **2007**, *40*, 1107−1121.

(5) Hodas, N.; Zuend, A.; Mui, W.; Flagan, R. C.; Seinfeld, J. H. Influence of Particle-Phase State on the Hygroscopic Behavior of Mixed Organic-Inorganic Aerosols. *Atmos. Chem. Phys.* **2015**, *15*, 5027−5045.

(6) Cotterell, M. I.; Willoughby, R. E.; Bzdek, B. R.; Orr-Ewing, A. J.; Reid, J. P. A Complete Parameterisation of the Relative Humidity and Wavelength Dependence of the Refractive Index of Hygroscopic Inorganic Aerosol Particles. *Atmos. Chem. Phys.* **2017**, *17*, 9837−9851.

(7) Abianeh, O. S.; Chen, C. P.; Mahalingam, S. Numerical Modeling of Multi-Component Fuel Spray Evaporation Process. *Int. J. Heat Mass Transfer* **2014**, *69*, 44−53.

(8) Nandiyanto, A. B. D.; Okuyama, K. Progress in Developing Spray-Drying Methods for the Production of Controlled Morphology Particles: From the Nanometer to Submicrometer Size Ranges. *Adv. Powder Technol.* **2011**, *22*, 1−19.

(9) Iskandar, F.; Gradon, L.; Okuyama, K. Control of the morphology of nanostructured particles prepared by the spray drying of a nanoparticle sol. *J. Colloid Interface Sci.* **2003**, *265*, 296−303.

(10) Bertrand, G.; Filiatre, C.; Mahdjoub, H.; Foissy, A.; Coddet, C. Influence of Slurry Characteristics on the Morphology of Spray-Dried Alumina Powders. *J. Eur. Ceram. Soc.* **2003**, *23*, 263−271.

(11) Shakiba, S.; Mansouri, S.; Selomulya, C.; Woo, M. W. The Role of the Intermediate Stage of Drying on Particle in-Situ Crystallization in Spray Dryers. *Powder Technol.* **2018**, *323*, 357−366.

(12) Hoe, S.; Ivey, J. W.; Boraey, M. A.; Shamsaddini-Shahrbabak, A.; Javaheri, E.; Matinkhoo, S.; Finlay, W. H.; Vehring, R. Use of a Fundamental Approach to Spray-Drying Formulation Design to Facilitate the Development of Multi-Component Dry Powder Aerosols for Respiratory Drug Delivery. *Pharm. Res.* **2013**, *31*, 449−465.

(13) Choudhury, M. D.; Dutta, T.; Tarafdar, S. Pattern Formation in Droplets of Starch Gels Containing NaCl Dried on Different Surfaces. *Colloids Surf., A* **2013**, *432*, 110−118.

(14) Erbil, H. Y. Evaporation of Pure Liquid Sessile and Spherical Suspended Drops: A Review. *Adv. Colloid Interface Sci.* **2012**, *170*, 67−86.

(15) Deegan, R. D.; Bakajin, O.; Dupont, T. F.; Huber, G.; Nagel, S. R.; Witten, T. A. Capillary Flow as the Cause of Ring Strins from Dried Liquid Drops. *Nature* **1997**, *389*, 827−829.

(16) Carruthers, A. E.; Reid, J. P.; Orr-Ewing, A. J. Longitudinal Optical Trapping and Sizing of Aerosol Droplets. *Opt. Express* **2010**, *18*, 14238−14244.

(17) Tang, I. N.; Munkelwitz, H. R. Water Activities, Densities, and Refractive Indices of Aqueous Sulfates and Sodium Nitrate Droplets of Atmospheric Importance. *J. Geophys. Res.: Atmos.* **1994**, *99*, 18801−18808.

(18) Schiffter, H.; Lee, G. Single-Droplet Evaporation Kinetics and Particle Formation in an Acoustic Levitator. Part 1: Evaporation of Water Microdroplets Assessed Using Boundary-Layer and Acoustic Levitation Theories. *J. Pharm. Sci.* **2007**, *96*, 2274−2283.

(19) Baldelli, A.; Boraey, M. A.; Nobes, D. S.; Vehring, R. Analysis of the Particle Formation Process of Structured Microparticles. *Mol. Pharm.* **2015**, *12*, 2562−2573.

(20) Sosnik, A.; Seremeta, K. P. Advantages and Challenges of the Spray-Drying Technology for the Production of Pure Drug Particles and Drug-Loaded Polymeric Carriers. *Adv. Colloid Interface Sci.* **2015**, *223*, 40−54.

(21) Sadek, C.; Schuck, P.; Fallourd, Y.; Pradeau, N.; Le Floch-Fouéré, C.; Jeantet, R. Drying of a single droplet to investigate process-structure-function relationships: a review. *Dairy Sci. Technol.* **2014**, *95*, 771−794.

(22) Vehring, R. Pharmaceutical Particle Engineering via Spray Drying. *Pharm. Res.* **2007**, *25*, 999−1022.

(23) Vehring, R.; Foss, W. R.; Lechuga-Ballesteros, D. Particle Formation in Spray Drying. *J. Aerosol Sci.* **2007**, *38*, 728−746.

(24) Osman, A.; Goehring, L.; Patti, A.; Stitt, H.; Shokri, N. Fundamental Investigation of the Drying of Solid Suspensions. *Ind. Eng. Chem. Res.* **2017**, *56*, 10506−10513.

(25) Lee, S.; Wi, H. S.; Jo, W.; Cho, Y. C.; Lee, H. H.; Jeong, S.-Y.; Kim, Y.-I.; Lee, G. W. Multiple Pathways of Crystal Nucleation in an Extremely Supersaturated Aqueous Potassium Dihydrogen Phosphate (KDP) Solution Droplet. *Proc. Natl. Acad. Sci. U.S.A.* **2016**, *113*, 13618−13623.

(26) Han, R. J.; Moss, O. R.; Wong, B. A. Derivation and Application of an Analytical Solution of the Mass Transfer Equation to the Case of Forced Convective Flow around a Cylindrical and a Spherical Particle with Fluid Surface Properties. *J. Aerosol Sci.* **1996**, *27*, 235−247.

(27) Na, H.-S.; Arnold, S.; Myerson, A. S. Cluster Formation in Highly Supersaturated Solution Droplets. *J. Cryst. Growth* **1994**, *139*, 104−112.

(28) Sear, R. P. Quantitative Studies of Crystal Nucleation at Constant Supersaturation: Experimental Data and Models. *CrystEngComm* **2014**, *16*, 6506−6522.

(29) Gao, Y.; Chen, S. B.; Yu, L. E. Efflorescence Relative Humidity of Airborne Sodium Chloride Particles: A Theoretical Investigation. *Atmos. Environ.* **2007**, *41*, 2019−2023.

(30) Cohen, M. D.; Flagan, R. C.; Seinfeld, J. H. Studies of Concentrated Electrolyte Solutions Using the Electrodynamic Balance. 1. Water Activities for Single-Electrolyte Solutions. *J. Phys. Chem.* **1987**, *91*, 4563−4574.

(31) Clegg, S. L.; Brimblecombe, P.; Wexler, A. S. Thermodynamic Model of the System H+−NH4+−Na+−SO42-−NO3-−Cl-−H2O at 298.15 K. *J. Phys. Chem. A* **1998**, *102*, 2155−2171.

(32) Tang, I.; Munkelwitz, H. An Investigation of Solute Nucleation in Levitated Solution Droplets. *J. Colloid Interface Sci.* **1984**, *98*, 430−438.

(33) Brandel, C.; ter Horst, J. H. Measuring Induction Times and Crystal Nucleation Rates. *Faraday Discuss.* **2015**, *179*, 199−214.

DOI: 10.1021/acs.jpcb.8b09584
J. Phys. Chem. B 2019, 123, 266−276

(34) Pradhan, T. K.; Panigrahi, P. K. Evaporation Induced Natural Convection inside a Droplet of Aqueous Solution Placed on a Superhydrophobic Surface. *Colloids Surf., A* **2017**, *530*, 1−12.
(35) WHO. Guideline: Sodium Intake for Adults and Children. *Nutrition*; World Health Organisation, 2012.
(36) Cho, H.-Y.; Kim, B.; Chun, J.-Y.; Choi, M.-J. Effect of Spray-Drying Process on Physical Properties of Sodium Chloride/maltodextrin Complexes. *Powder Technol.* **2015**, *277*, 141−146.
(37) Chindapan, N.; Niamnuy, C.; Devahastin, S. Physical Properties, Morphology and Saltiness of Salt Particles as Affected by Spray Drying Conditions and Potassium Chloride Substitution. *Powder Technol.* **2018**, *326*, 265−271.
(38) Li, X.; Gupta, D.; Eom, H.-J.; Kim, H.; Ro, C.-U. Deliquescence and Efflorescence Behavior of Individual NaCl and KCl Mixture Aerosol Particles. *Atmos. Environ.* **2014**, *82*, 36−43.
(39) Davies, J. F.; Haddrell, A. E.; Reid, J. P. Time-Resolved Measurements of the Evaporation of Volatile Components from Single Aerosol Droplets. *Aerosol Sci. Technol.* **2012**, *46*, 666.
(40) Cai, C.; Miles, R. E. H.; Cotterell, M. I.; Marsh, A.; Rovelli, G.; Rickards, A. M. J.; Zhang, Y.-h.; Reid, J. P. Comparison of Methods for Predicting the Compositional Dependence of the Density and Refractive Index of Organic-Aqueous Aerosols. *J. Phys. Chem. A* **2016**, *120*, 6604−6617.
(41) Olsen, A. P.; Flagan, R. C.; Kornfield, J. A. Single-Particle Levitation System for Automated Study of Homogeneous Solute Nucleation. *Rev. Sci. Instrum.* **2006**, *77*, 073901−073908.
(42) Vortisch, H.; Kramer, B.; Weidinger, I.; Woeste, L.; Leisner, T.; Schwell, M.; Baumgaertel, H.; Ruehl, E. Homogeneous Freezing Nucleation Rates and Crystallization Dynamics of Single Levitated Sulfuric Acid Solution Droplets. *Phys. Chem. Chem. Phys.* **2000**, *2*, 1407−1413.
(43) Biskos, G.; Malinowski, A.; Russell, L. M.; Buseck, P. R.; Martin, S. T. Nanosize Effect on the Deliquescence and the Efflorescence of Sodium Chloride Particles. *Aerosol Sci. Technol.* **2006**, *40*, 97−106.
(44) Durán-Olivencia, M. A.; Otálora, F. A Brownian Model for Crystal Nucleation. *J. Cryst. Growth* **2013**, *380*, 247−255.
(45) *CRC Handbook of Chemistry and Physics*; Rumble, J. R., Ed.; CRC Press, Taylor & Francis Group: Boca Raton, 2013.
(46) Power, R. M.; Simpson, S. H.; Reid, J. P.; Hudson, A. J. The Transition from Liquid to Solid-like Behaviour in Ultrahigh Viscosity Aerosol Particles. *Chem. Sci.* **2013**, *4*, 2597−2604.
(47) Kulmala, M.; Vesala, T.; Wagner, P. E. An Analytical Expression For the Rate of Binary Condensational Particle Growth. *Proc. R. Soc. London, Ser. A* **1993**, *441*, 589−605.
(48) Crank, J.; Nicolson, P.; Hartree, D. R. A Practical Method for Numerical Evaluation of Solutions of Partial Differential Equations of the Heat-Conduction Type. *Math. Proc. Cambridge Philos. Soc.* **1947**, *43*, 50−67.
(49) Desarnaud, J.; Derluyn, H.; Carmeliet, J.; Bonn, D.; Shahidzadeh, N. Metastability Limit for the Nucleation of NaCl Crystals in Confinement. *J. Phys. Chem. Lett.* **2014**, *5*, 890−895.
(50) Tang, I. N.; Munkelwitz, H. R.; Wang, N. Water activity measurements with single suspended droplets: The NaCl-H2O and KCl-H2O systems. *J. Colloid Interface Sci.* **1986**, *114*, 409−415.
(51) Utoft, A.; Kinoshita, K.; Bitterfield, D. L.; Needham, D. Manipulating Single Microdroplets of NaCl Solutions: Solvent Dissolution, Microcrystallization, and Crystal Morphology. *Langmuir* **2018**, *34*, 3626−3641.
(52) Krieger, U. K.; Marcolli, C.; Reid, J. P. Exploring the Complexity of Aerosol Particle Properties and Processes Using Single Particle Techniques. *Chem. Soc. Rev.* **2012**, *41*, 6631−6662.
(53) Clegg, S. L.; Wexler, A. S. Densities and Apparent Molar Volumes of Atmospherically Important Electrolyte Solutions. 1. The Solutes H2SO4, HNO3, HCl, Na2SO4, NaNO3, NaCl, (NH4)2SO4, NH4NO3, and NH4Cl from 0 to 50 °C, Including Extrapolations to Very Low Temperature and to the Pure Liquid State, and NaHSO4, NaOH, and NH3at 25 °C. *J. Phys. Chem. A* **2011**, *115*, 3393−3460.
(54) Baldelli, A.; Vehring, R. Control of the radial distribution of chemical components in spray-dried crystalline microparticles. *Aerosol Sci. Technol.* **2016**, *50*, 1130−1142.
(55) Hu, H.; Larson, R. G. Analysis of the Effects of Marangoni Stresses on the Microflow in an Evaporating Sessile Droplet. *Langmuir* **2005**, *21*, 3972−3980.
(56) Holländer, W.; Windt, H. Forces upon Droplets Induced by External and Internal Concentration Gradients. *J. Aerosol Sci.* **1994**, *25*, S351−S352.
(57) Kim, I.; Kihm, K. D. Unveiling Hidden Complex Cavities Formed during Nanocrystalline Self-Assembly. *Langmuir* **2009**, *25*, 1881−1884.

DOI: 10.1021/acs.jpcb.8b09584
J. Phys. Chem. B 2019, 123, 266−276